Mechanism and Machine Theory 74 (2014) 337–353

Contents lists available at ScienceDirect

Mechanism and Machine Theory

journal homepage: www.elsevier.com/locate/mechmt

# A novel leg orthosis for lower limb rehabilitation robots of the sitting/lying type

Weiqun Wang, Zeng-Guang Hou *, Lina Tong, Feng Zhang, Yixiong Chen, Min Tan

*State Key Laboratory of Management and Control for Complex Systems, Institute of Automation, Chinese Academy of Sciences, Beijing 100190, China*

ARTICLE INFO

*Article history:*
Received 16 November 2012
Received in revised form 23 December 2013
Accepted 28 December 2013
Available online 23 January 2014

*Keywords:*
Rehabilitation robot
Leg orthosis
Optimization
Kinematics

ABSTRACT

This paper proposes a novel leg orthosis for lower limb rehabilitation robots of the sitting/lying type. It consists of three joint mechanisms: hip, knee and ankle, and two sets of links: thigh and crus. Each driving motor is located close to the associated joint and the rotational axis of each joint mechanism is unique and stable. These features make it outperform the similar mechanisms in stability and dynamic performance. Different forms of eccentric slider-crank mechanisms are applied in the three joint mechanisms, respectively, such that they can be optimized independently. The optimization problems for the hip and knee joint mechanisms, characterized as strongly nonlinear, are developed respectively. Then, a particle swarm optimization algorithm is used to obtain the optimal solutions, which are subsequently validated by comprehensive comparisons. Moreover, the kinematics necessary for motion control and trajectory tracking are investigated, which denote the relationships between the displacements and velocities of the joint mechanisms, lead screws and the end effector. Finally, this paper illustrates the feasibility of the application of the leg orthosis to actual rehabilitation exercises by a simulation example.



## 1. Introduction

Stroke is one of the leading causes of death and disability worldwide, and the number of patients with stroke is still increasing [1,2]. For SCI[1], reported incidence lies between 10.4 and 83 per million inhabitants per year in the decade before 2006 [3], and now the annual incidence of traumatic SCI worldwide is estimated to be 35 patients per million [4]. Neurological impairment, frequently caused by stroke, SCI and other neurological disorders, often leads to limb dysfunctions, especially paraplegia and hemiplegia. Although it has been proven that repetitive and intensive rehabilitation exercises with the disabled limbs were effective to neurorehabilitation and motor recovery [5,6], the conventional lower limb rehabilitation exercises are labor intensive and expensive, which limit its clinical application and effects. Therefore, more and more LLRR[2] with novel rehabilitation tools have been designed.

LLRR can be categorized into two types according to the postures of the patients doing exercises with them. One is the sitting/lying type, which is used by patients while sitting or lying, e.g. MotionMaker (Swortec, Switzerland) [7] and Lambda [8]; the other is the standing/walking type, which is used by patients in standing or walking postures and usually incorporated with BWS[3] system, e.g. Lokomat [9], LokoHelp (LokoHelp Group, Germany) [10], and WalkTrainer (Swortec, Switzerland) [11]. Although none of the two types has overwhelming superiority, the sitting/lying type has been less studied presently. However, the sitting and lying postures are closer to those used by physicians or therapists when they are evaluating the motor functions of patients with lower limb dysfunctions, especially those with paraplegia or hemiplegia. Moreover, compared with the standing/walking type, the sitting/lying

* Corresponding author. Tel./fax: +86 10 8254 4531.
*E-mail address:* hou@compsys.ia.ac.cn (Z.-G. Hou).

[1] SCI: Spinal cord injury.
[2] LLRR: Lower limb rehabilitation robots.
[3] BWS: Body weight support.

0094-114X/$ – see front matter © 2014 Elsevier Ltd. All rights reserved.
http://dx.doi.org/10.1016/j.mechmachtheory.2013.12.021

type is easier to use for patients and therapists or nurses from the beginning to the mid of the long term rehabilitation when the patients cannot stand with their weak lower limbs. Therefore, this research focuses on the LLRR of the sitting/lying type.

This kind of robots conventionally consists of one chair and two leg orthoses, which are the most complicated and important parts of these robots and can be synthesized by using different kinds of mechanisms. In [12], mechanical links were used to produce the multi-joint motions. In order to obtain an ideal impedance control system, the device was connected to the patient using elastic components. The disadvantage of this device is, it cannot be used for active exercises that involve the voluntary participation of patients and have been proven more effective for neurorehabilitation and motor recovery [13]. In the design proposed in [14], timing belts were used and the axes of the belt wheels were stable and could exactly match those of human leg joints. Unfortunately, in this design, harmonic speed reducers were used to obtain high transmission ratios for the hip and knee joints, which together with the driving motors were difficult to be located close to associated joints because of the large dimensions. Therefore, the timing belts were long and thus vibration would be caused inevitably when the mechanism was running. In [7], the crank system activated by a lead screw was used to match the motion of each human leg joint. DC motors were located close to associated joints and lead screws could produce high precision; hence, this mechanism was relatively stable. However, the knee joint mechanism could induce a sliding instantaneous center of rotation and a slight movement of the sagittal plane [7]. Moreover, it was shown in Fig. 3 of [15] and Fig. 1 of [23], the torque–angle characteristics of the knee joint mechanism were different from that of human knee joint. Finally, the hip, knee and ankle joints were designed by using the same form of mechanisms in this device [15]. Whereas, angle ranges of the hip and ankle joints are smaller and the torque–angle characteristics of human hip and ankle joints are different from that of knee joint. Therefore, mechanical characteristics of the hip and ankle joint mechanisms proposed in [7] might have been better if they had been designed by using different forms of mechanisms.

Besides, other mechanisms also can be used to replace leg orthoses, such as the mechanisms proposed in [8,16]. However, in these mechanisms, the motion of human foots was limited to a horizontal or sloping plane, thus the exercises they provided were relatively simple.

In this paper, a novel leg orthosis is proposed to overcome the deficiencies of the existing leg orthoses for LLRR of the sitting/lying type. This orthosis consists of three joint mechanisms, corresponding to hip, knee and ankle joints of human leg, respectively, and two sets of links, corresponding to human thigh and crus, respectively. ESCM[4] is used in each joint mechanism to convert the rotation of driving motor, which is with high rotational velocity and lower torque, into the rotation of associated joint, which is with lower rotational velocity and higher torque. A high ratio of the rotational velocity of driving motor to that of the associated joint is obtained by using a lead screw and optimizing the dimensions for each joint mechanism. Hence, there is no need to include additional speed reducing systems. This feature makes it possible to locate the driving motor close to the associated joint, consequently, the transmission system can be simplified to obtain higher stability. The lengths of the thigh and crus of the orthosis can be adjusted, respectively, and each of the hip, knee and ankle joints has unique and stable rotational axis. Therefore, each of the rotational axes of the hip, knee and ankle joints can be adjusted to accurately match that of corresponding human leg joint, which helps to make the process of rehabilitation exercises more comfortable.

For actual application of the leg orthosis proposed in this paper, the following conditions should be satisfied: 1) the dimensions of the leg orthosis should be smaller for the convenience of application; 2) the joint angle and output torque of each joint mechanism should be designed in reasonable ranges; 3) the transmission ratio of each joint mechanism should be higher to obtain greater output torque of associated joint by using a low power DC motor; 4) the relationship between output torque and joint angle for each joint mechanism should be suitable for rehabilitation exercises. Conventionally, mechanisms can be synthesized by trials if the requirements are relatively simple. However, in this design, the first three conditions are contradictory to each other and the last one is difficult to be described in math, and as a result, it is hard to obtain the mechanisms satisfying the above conditions by conventional methods. Therefore, in this paper, the leg orthosis is designed in this way: the first three conditions are applied to develop the optimization problems for associated mechanisms and the last one is used as validation.

The optimization problems developed in this paper are strongly nonlinear, which is shown in Subsections 2.2 and 2.3. Therefore, a PSO[5] method [17], which has been proven effective and easier to use in solving nonlinear optimization problems by plenty of applications [18–20], is used to obtain the optimal solutions. Then, comparisons, including that between the optimized and unoptimized mechanisms and that between the torque–angle characteristics of the knee joint mechanism and of human knee joint, are detailed to validate the optimization results and the suitableness for actual rehabilitation exercises. Moreover, the kinematics, necessary for motion control and trajectory tracking, are obtained by taking the leg orthosis as a linkage with two links. Finally, by using the optimized dimensions and the kinematics obtained in this paper, a simulation example is formulated to demonstrate the feasibility of the application to actual lower limb rehabilitation exercises.

The remainder of the paper is organized as follows: Section 2 describes the mechanism synthesis and optimization in detail. The kinematics are analyzed in Section 3. Section 4 introduces a simulation example and a small discussion is presented. This paper is concluded in Section 5.

## 2. Synthesis and optimization

The leg orthosis proposed in this paper is designed for people with height from 1500 mm to 1900 mm. According to the respective proportion of thigh and crus lengths and ankle height to body height [21], the length ranges of three parts of the orthosis are given in

[4] ESCM: Eccentric slider-crank mechanism.
[5] PSO: Particle swarm optimization.

Table 1. By considering the actual application, the angle range and the maximal torque for each joint are given in Table 2. As the knee and ankle joint mechanisms of this orthosis are similar, the synthesis and optimization are formulated by focusing on the hip and knee joint mechanisms, and the optimal dimensions for the ankle joint can be obtained by the same methods.

### 2.1. The leg orthosis

The virtual prototype of the leg orthosis proposed in this paper is shown in Fig. 1. It consists of three joint mechanisms, corresponding to hip, knee and ankle joints of human leg, respectively, and two sets of links, corresponding to human thigh and crus, respectively.

The hip joint mechanism is built directly on the base. Both the thigh and crus consist of two links, i.e. thigh links 1 and 2 and crus links 1 and 2. Every adjacent two of the five parts: the thigh, crus and the hip, knee and ankle joints, are linked to each other to form the leg-like mechanism. ESCM is used in each joint mechanism. The lead screw and associated screw nut can be taken as a sliding pair for simplification, where the former is taken as a sliding bar. Each screw nut can be driven by a DC motor through a timing belt and can rotate relatively to the base. Meanwhile, the associated lead screw cannot rotate but translate, which leads to variation of the angle between the two links constituting a revolution pair at each joint. These angles are used to match those of corresponding human leg joints.

By using the lead screw and optimizing the dimensions, each joint mechanism can produce a high transmission ratio, which is detailed in Subsection 2.2, and high precision. As the hip, knee and ankle joint mechanisms are driven by associated DC motors respectively, they can be controlled separately or simultaneously. Thus, this leg orthosis can be used to provide both single joint and multiple joint exercises. Position and force sensors are mounted in each joint mechanism to obtain the information needed for both safety reasons and motion control. Furthermore, by using the measurements obtained from these sensors, the motion intention of the patient doing exercises with the orthosis can be recognized, such that the leg orthosis can be used to provide passive and active exercises as well. Besides, lengths of the thigh and crus and height of the ankle can be adjusted with hand wheels 1, 2 and 3, respectively, and each of the hip, knee and ankle joints has unique and stable rotational axis. Therefore, the rotational axes of the hip, knee and ankle joints of the mechanisms can be adjusted to exactly match those of corresponding human leg joints, which helps to make the process of rehabilitation exercises more comfortable.

### 2.2. Synthesis and optimization of the hip joint mechanism

The details of the hip joint are shown in Fig. 2(a), where auxiliary parts without relation to the kinematics are not included. Hip links 1 and 2 are fixed on the base. Screw nut 1 is fixed on its base which is connected to hip link 2 at joint $A_1$, hence it can rotate relatively to hip link 2. Lead screw 1 and screw nut 1 constitute a helix pair, through which the rotation of screw nut 1 is converted into the translational motion of lead screw 1. Lead screw 1 and force sensor 1 are fixed on the base of force sensor 1. Every adjacent two of the three parts: the base of force sensor 1, thigh link 1 and hip link 1, constitute revolution pairs at joint $B_1$ and the hip joint, respectively. When screw nut 1 is driven by DC motor 1 through timing belt 1 and rotates, lead screw 1 will translate relatively to screw nut 1. Meanwhile, each two parts connected at the three joints (joints $A_1$ and $B_1$ and the hip joint), will rotate relatively to each other, which immediately leads to variation of the angle between hip link 1 and thigh link 1. In this mechanism, the hip joint corresponds to hip joint of human leg and the angle between hip link 1 and thigh link 1 is used to match human hip angle.

The ratio of the torque of screw nut 1 to that of DC motor 1 is determined by the diameters of associated belt wheels. The output torque of the hip joint is determined by the force along lead screw 1 and the distance between the hip joint and lead screw 1. Therefore, when the transmission loss and mass of the mechanism are not considered, the output torque of the hip joint can be formulated as follows:

$$\tau_{hip} = 2\pi\tau_{motor} r_{belt} d_1 / e \tag{1}$$

where $\tau_{hip}$ and $\tau_{motor}$ are the output torques of the hip joint and DC motor 1, respectively; $r_{belt}$ denotes the ratio between the diameters of the belt wheels connected respectively to screw nut 1 and DC motor 1; $d_1$ is the distance between the hip joint and lead screw 1, which varies with the angle of hip joint; $e$ is the lead of lead screw 1. Hence, the ratio of output torque of the hip joint to that of DC motor 1 can be described by:

$$r_{hip} = 2\pi r_{belt} d_1 / e. \tag{2}$$

It is shown in Eq. (2) that a higher transmission ratio of the mechanism can be obtained by designing bigger $r_{belt}$ and $d_1$ and choosing smaller $e$. For example, if $r_{belt} = 2$, $d_1 \geq 150$ mm and $e = 5$ mm, and when other factors are not considered, the

**Table 1**
The length ranges of three parts of the leg orthosis.

| | Thigh length | Crus length | Ankle height |
|---|---|---|---|
| Minimum (mm) | 305 | 325 | 60 |
| Maximum (mm) | 395 | 420 | 90 |

**Table 2**
The design parameters of three joints.

| | Hip | Knee | Ankle |
|---|---|---|---|
| Minimal angle (°) | 0 | −130 | −30 |
| Maximal angle (°) | 70 | −10 | 30 |
| Maximal torque (Nm) | 150 | 65 | 5 |

transmission ratio will be greater than 377. That means the DC motor 1 can be selected as with higher rotational velocity and lower output torque to obtain lower rotational velocity and higher output torque of the hip joint, which is similar to the characteristics of human hip joint. The design of $r_{belt}$ is simple by designing the ratio between the diameters of associated timing belt wheels and $e$ is limited to several values. Whereas, the minimal value of $d_1$, which should be as big as possible to obtain a higher transmission ratio, varies with the dimensions of the mechanism; hence, the design of $d_1$ is relatively difficult but necessary for obtaining a higher transmission ratio, as is shown in Eq. (2). Therefore, the synthesis and optimization of the hip joint mechanism mainly focus on finding the dimensions for which the minimal value of $d_1$ is bigger. As described in Section 1, the requirements for the dimension and the hip joint angle are considered in the optimization, and the torque–angle characteristics of the hip joint mechanism are used to validate the optimal solution.

The schematic plot of the hip joint mechanism is given in Fig. 2(b), where revolution pairs at points $A_1$, $B_1$ and $C_1$ represent joints $A_1$, $B_1$ and the hip joint, respectively. Links $D_1C_1$ and $C_1E_1$ are collinear and the angle between links $B_1D_1$ and $D_1C_1$ is designed to be 110° in this mechanism; hence, the distance of points $B_1$ and $C_1$ (i.e. $r_1$) and the angle between links $C_1E_1$ and $B_1C_1$ (i.e. $\beta_1$) determine uniquely the lengths of links $B_1D_1$ and $D_1C_1$. The helix pair constituted by lead screw 1 and screw nut 1 is treated as a sliding pair for simplification. It is shown in Fig. 2(b), this mechanism can be determined by $r_1$, $\beta_1$ and the relative position of points $A_1$ to $C_1$ (i.e. $a_1$ and $b_1$, for the horizontal and vertical distance, respectively). Therefore, the minimal value of $d_1$ is determined by $r_1$, $a_1$, $b_1$ and $\beta_1$ as well. A vector loop equation can be obtained from Fig. 2(b) as follows:

$$\boldsymbol{R}_{11} = \boldsymbol{R}_{12} + \boldsymbol{R}_{13}. \tag{3}$$

The $x$ and $y$ components, respectively, are:

$$x_{B_1} = a_1 + r_1 \cos\left(\beta_1 + \theta_{hip}\right), y_{B_1} = b_1 + r_1 \sin\left(\beta_1 + \theta_{hip}\right) \tag{4}$$

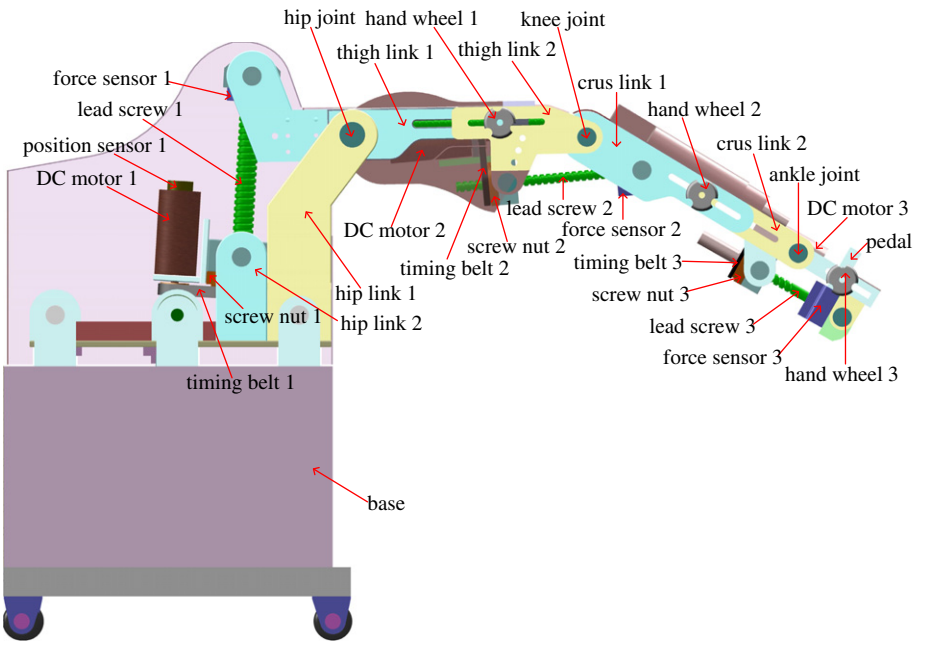


**Fig. 1.** The virtual prototype of the leg orthosis.

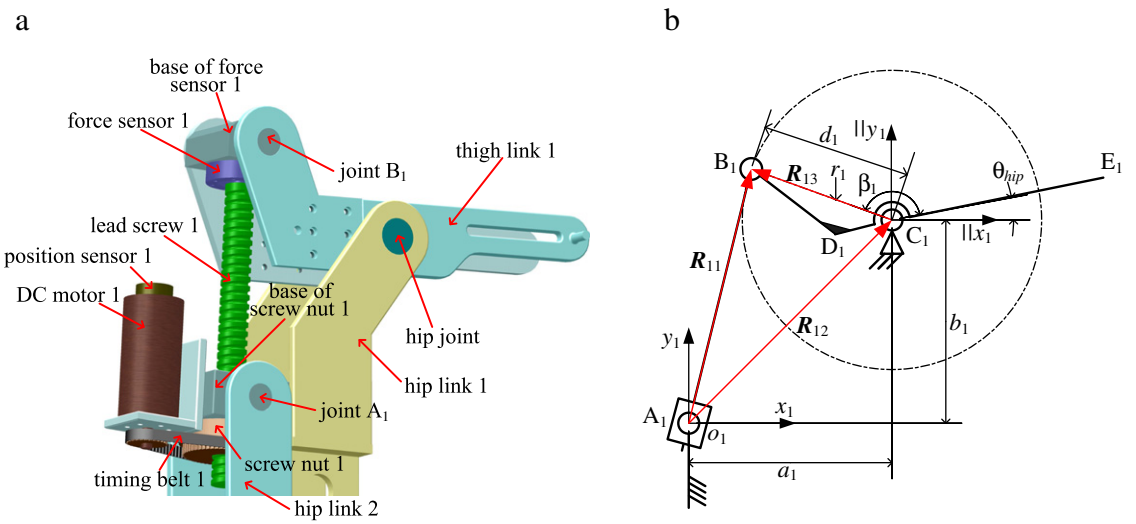


**Fig. 2.** (a) The details and (b) schematic plot of the hip joint mechanism. $||x_1$ and $||y_1$ signify axes that are parallel to $o_1x_1$ and $o_1y_1$, respectively.

where $\theta_{hip}$ represents the hip joint angle. The equation of line $A_1B_1$ and the distance between point $C_1$ and line $A_1B_1$ can be obtained, respectively, as follows:

$$y_{B_1}x - x_{B_1}y = 0 \tag{5}$$

and

$$d_1 = \frac{y_{B_1}a_1 - x_{B_1}b_1}{\sqrt{x_{B_1}^2 + y_{B_1}^2}}. \tag{6}$$

The dead points, where $d_1 = 0$, should be avoided and point $B_1$ should stay left to line $A_1C_1$ when the hip joint angle varies in the range given in Table 2, therefore, the following constraint can be obtained:

$$d_1 > 0, \forall\theta_{hip} \in [0^\circ, 70^\circ]. \tag{7}$$

The minimum of $d_1$ when link $C_1E_1$ rotates about point $C_1$ should be subject to the constraint as follows:

$$d_{min}^{hip} \le d_1, \forall\theta_{hip} \in [0^\circ, 70^\circ] \tag{8}$$

where $d_{min}^{hip}$ is the minimum of $d_1$. To make $d_{min}^{hip}$ as big as possible and by considering Eqs. (4)–(8), the design variables with their ranges, the objective function, and the constraints can be obtained as follows:

Design vector:

$$\begin{aligned} &\boldsymbol{X}_{hip} = (a_1, b_1, r_1, \beta_1) \\ &a_1 \in [a_{11}, a_{12}], b_1 \in [b_{11}, b_{12}], r_1 \in [r_{11}, r_{12}], \beta_1 \in [\beta_{11}, \beta_{12}] \end{aligned} \tag{9}$$

Objective function to be maximized:

$$F_1\left(\boldsymbol{X}_{hip}\right) = d_{min}^{hip} \tag{10}$$

Constraints to be satisfied:

$$d_{min}^{hip} \le \frac{y_{B_1}a_1 - x_{B_1}b_1}{\sqrt{x_{B_1}^2 + y_{B_1}^2}}, d_{min}^{hip} > 0, \forall\theta_{hip} \in [0^\circ, 70^\circ] \tag{11}$$

where $x_{B_1}$ and $y_{B_1}$ are defined by Eq. (4), and $[a_{11},a_{12}]$, $[b_{11},b_{12}]$, $[r_{11},r_{12}]$ and $[\beta_{11},\beta_{12}]$ should be set according to actual dimensions of the mechanism.

It is shown above that the optimization problem is strongly nonlinear. Therefore, a PSO algorithm, which is effective and easy to use for solving nonlinear problems, is applied in this design. The PSO algorithm is a global optimization and evolutionary computation technique developed by Kennedy and Eberhart [17,22], inspired by social behavior of bird flocking. Evolutionary algorithms like PSO are often more effective for solving nonlinear optimization problems than traditional deterministic algorithms which often become trapped in local minima [18]. Moreover, compared with GA[6], the most commonly used nontraditional optimization technique, the PSO algorithm does not need complex encoding and decoding process and special genetic operator but requires less number of iterations for convergence to the optimal solution [19]. Plenty of applications of PSO have been presented since its introduction. In [19], a PSO algorithm was used to find the optimal combination of design parameters for minimal weight of a spur gear train, where it was shown that the PSO algorithm offered better gear design solutions than GA. In [18], a PSO algorithm was used to develop a general Grashof four-bar mechanism synthesis routine, where the accurate solution and improved performance were obtained. In [20], the PSO algorithm was used to solve the optimization problem for hydro-mechanical power split transmissions, which showed a good convergence speed and the ability to overcome local minima. However, for optimization of ESCM, there is little effort to apply this method. Therefore, a trial application of the PSO method to optimization of ESCM is carried out in this paper.

In a PSO algorithm, particles representing search-variable sets move through the problem space and share information with the swarm regarding their fitness. Let $m$ and $d$ be the number of particles and the dimension of each particle, respectively, the update of each particle can be accomplished by the following equations:

$$\boldsymbol{V}_{j,i+1} = w_i \boldsymbol{V}_{j,i} + c_1 r_{j,i,1}\left(\boldsymbol{pBest}_{j,i} - \boldsymbol{X}_{j,i}\right) + c_2 r_{j,i,2}\left(\boldsymbol{gBest}_i - \boldsymbol{X}_{j,i}\right) \tag{12}$$

$$\boldsymbol{X}_{j,i+1} = \boldsymbol{X}_{j,i} + \boldsymbol{V}_{j,i+1} \tag{13}$$

where $\boldsymbol{V}_{j,i+1}$, $\boldsymbol{V}_{j,i}$, $\boldsymbol{pBest}_{j,i}$, $\boldsymbol{gBest}_i$, $\boldsymbol{X}_{j,i}$ and $\boldsymbol{X}_{j,i+1} \in \boldsymbol{R}^d$; $j \in [0,m]$. $\boldsymbol{V}_{j,i+1}$ denotes a new velocity vector for the $j$th particle based on its previous velocity $\boldsymbol{V}_{j,i}$, previous position $\boldsymbol{X}_{j,i}$, the best location $\boldsymbol{pBest}_{j,i}$ it has achieved so far, and the global best location $\boldsymbol{gBest}_i$ the population has achieved [19]. $w_i$, the inertia weight, is employed to control the exploration ability of the swarm. $c_1$ and $c_2$ are the acceleration constants, which represent effects of $\boldsymbol{pBest}_{j,i}$ and $\boldsymbol{gBest}_i$, respectively. $r_{j,i,1}$ and $r_{j,i,2}$ are the two random numbers independently generated in the range [0, 1] for the $j$th particle. Eq. (13) is used to update the position of the $j$th particle.

In this paper, in order to obtain better convergence performance and higher precision, the following inertia weight is used:

$$w_i = w_{max} - (w_{max} - w_{min})i/c_{loop} \tag{14}$$

where $w_{max}$, $w_{min}$ and $c_{loop}$ are the constants and denote the maximal and minimal values of inertia weight and the maximum of iteration number, respectively; $i$ is the iteration number.

For the optimization problem defined by Eqs. (9)–(11), the $j$th particle can be defined as:

$$\boldsymbol{X}_j = \left(x_{j,1}, x_{j,2}, x_{j,3}, x_{j,4}\right) \tag{15}$$

where $x_{j,1} \in [a_{11}.a_{12}]$, $x_{j,2} \in [b_{11},b_{12}]$, $x_{j,3} \in [r_{11},r_{12}]$ and $x_{j,4} \in [\beta_{11},\beta_{12}]$ represent, respectively, $a_1$, $b_1$, $r_1$ and $\beta_1$. The initial values of elements of $X_j$ are given by:

$$x_{j,0}^d = r_{j,0}^d\left(x_{max}^d - x_{min}^d\right) + x_{min}^d, d = 1,2,3,4 \tag{16}$$

where $x_{j,0}^d$, $r_{j,0}^d$, $x_{max}^d$, and $x_{min}^d$ are, respectively, the initial value, a random number generated in the range [0, 1], the maximal and minimal values of the $d$th element of the $j$th particle. The values of elements of $\boldsymbol{X}_j$ and $\boldsymbol{V}_j$ are restricted in the same ranges as $a_1$, $b_1$, $r_1$ and $\beta_1$, respectively. Initial values of the elements of velocity vector $\boldsymbol{V}_{j,0}$ are obtained by:

$$v_{j,0}^d = r_j^d\left(x_{max}^d - x_{min}^d\right) + x_{min}^d, d = 1,2,3,4 \tag{17}$$

where $v_{j,0}^d$ and $r_j^d$ are, respectively, the initial value of the $d$th element of $\mathbf{V}_{j,0}$ and a random number generated in the range [0, 1].

In the optimization, the ranges of variables $a_1$, $b_1$, $r_1$ and $\beta_1$ are given by:

$$a_1 \in [150,200], b_1 \in [150,200], r_1 \in [150,200], \beta_1 \in \left[110^\circ, 180^\circ\right]. \tag{18}$$

[6] GA: The genetic algorithm.

Other parameters of the PSO algorithm are given by:

- Maximum of iteration number: 1000;
- Population: 20;
- Maximum of the inertia weight: 0.95;
- Minimum of the inertia weight: 0.4;
- $c_1$ and $c_2$: 2.

It is shown in the computation process, this algorithm requires fewer than 1000 iterations to convergence to the optimal solutions, specifically, it often requires only about 300 iterations. However, if a traverse algorithm is used, the iteration number will be much higher. For example, if points in the ranges of $a_1$, $b_1$, $r_1$, and $\beta_1$, are chosen every other 1 mm or 1° for computation, the iteration number will be bigger than 8,750,000. Therefore the PSO algorithm is more effective for the optimization problem defined by Eqs. (9)–(11).

There are many optimal solutions that can be obtained by trials. Finally, a solution with small dimensions is used in the design, which is: $a_1 = 150$ mm, $b_1 = 158$ mm, $r_1 = 200$ mm and $\beta_1 = 150°$. The torque–angle characteristics of the hip joint mechanisms with the optimized and unoptimized dimensions are given in Fig. 3(a) and (b), respectively, where the forces along lead screw 1 are set to be 1000 N and the mass of the mechanism is not considered. It is shown that after optimization the minimum of output torque of the mechanism increases significantly, and at the same time, the variation range of the output torque when the hip joint angle varies from 0° to 70° decreases. That feature is helpful for DC motor 1 being smaller and the mechanism to run smoothly.

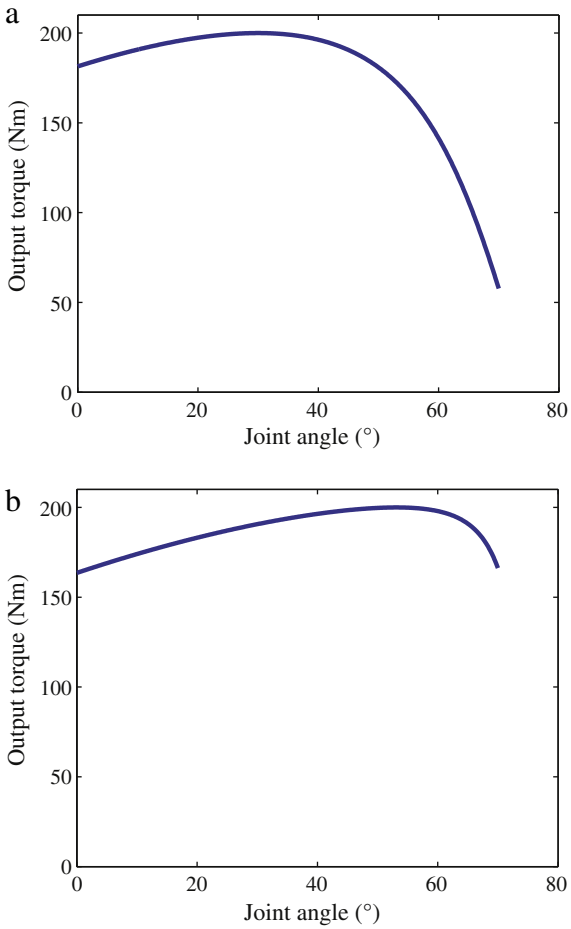


**Fig. 3.** The torque–angle characteristics of the hip joint mechanism with (a) unoptimized dimensions: $a_1 = 200$ mm, $b_1 = 200$ mm, $r_1 = 200$ mm and $\beta_1 = 150°$, and (b) optimized dimensions: $a_1 = 150$ mm, $b_1 = 158$ mm, $r_1 = 200$ mm and $\beta_1 = 150°$, respectively. The minimal torques are 57.7 Nm and 163.55 Nm for (a) and (b), respectively.

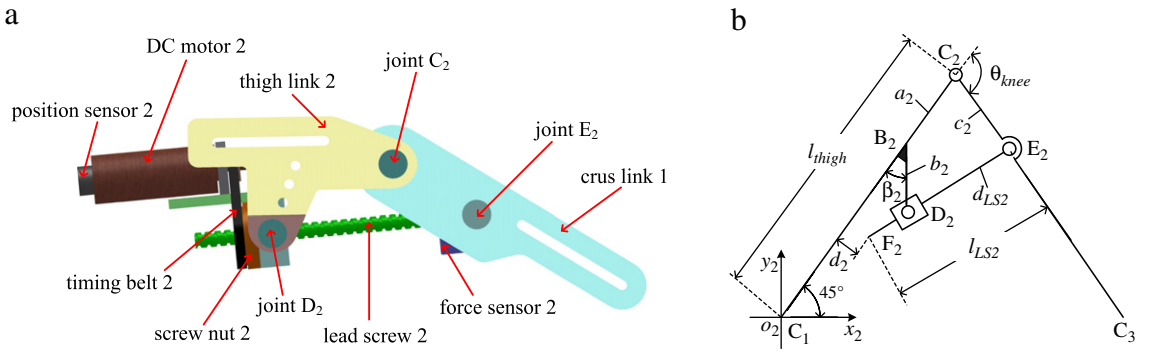


**Fig. 4.** (a) The details and (b) schematic plot of the knee joint mechanism.

### *2.3. Synthesis and optimization of the knee joint mechanism*

The knee joint mechanism, consisting of an ESCM, is shown in Fig. 4(a). Lead screw 2 and screw nut 2 constitute a helix pair. Every adjacent two of the four parts: screw nut 2, thigh link 2, crus link 1 and lead screw 2, constitute revolution pairs, respectively. When screw nut 2 is driven by DC motor 2 through timing belt 2 and rotates, lead screw 2 will undergo translational motion, which will lead to change of the angle between thigh link 2 and crus link 1. In this mechanism, the knee joint is used to match human knee joint and the angle between thigh link 2 and crus link 1 is taken as the knee joint angle (i.e. $\theta_{knee}$).

The schematic plot of the knee joint mechanism is given in Fig. 4(b), where the helix pair constituted by lead screw 2 and screw nut 2 is treated as a sliding pair which consists of sliding bar $E_2F_2$ and the slider at point $D_2$. Links $C_1C_2$ and $C_2C_3$ represent the centerline of the thigh mechanism between the knee and hip joints and the centerline of the crus mechanism between the knee and ankle joints, respectively. Revolution pairsat points $C_2$, $D_2$ and $E_2$ represent the knee joint and joints $D_2$ and $E_2$, respectively.

In Fig. 4(b), the angle between $x_2$-axis and link $C_1C_2$ is set to be 45°, and $l_{thigh}$, corresponding to the length of the thigh mechanism, is set to be 400 mm according to actual dimension. By considering the angle range of the knee joint, the length of lead screw 2 is set to be 270 mm in the design. It is shown that the knee joint mechanism is defined by lengths of links $B_2C_2$, $B_2D_2$ and $C_2E_2$ and the angle between links $B_2D_2$ and $C_1C_2$, i.e. $a_2$, $b_2$, $c_2$ and $\beta_2$, respectively. For the simplicity of optimization, $c_2$ is set to be 100 mm, which should be modified if the torque–angle characteristics of the optimized mechanism are inappropriate, and $a_2$, $b_2$ and $\beta_2$ are treated as parameters to be optimized. Therefore, the following equations can be obtained by the above discussion:

$$l_{thigh} = 400, c_2 = 100, l_{LS2} = 270. \tag{19}$$

The coordinate values of points $B_2$, $C_2$, $D_2$ and $E_2$ can be calculated, respectively, by:

$$x_{B_2} = \frac{l_{thigh} - a_2}{\sqrt{2}}, y_{B_2} = x_{B_2} \tag{20}$$

$$x_{C_2} = \frac{l_{thigh}}{\sqrt{2}}, y_{C_2} = x_{C_2} \tag{21}$$

$$x_{D_2} = x_{B_2} + b_2 \sin(\beta_2 - 45), y_{D_2} = y_{B_2} - b_2 \cos(\beta_2 - 45) \tag{22}$$

and

$$x_{E_2} = x_{C_2} + c_2 \cos(\theta_{knee} + 45), y_{E_2} = y_{C_2} + c_2 \sin(\theta_{knee} + 45). \tag{23}$$

Let

$$k_2 = \frac{y_{E_2} - y_{D_2}}{x_{E_2} - x_{D_2}}. \tag{24}$$

The coordinate values of point $F_2$ can be described by:

$$x_{F_2} = x_{E_2} - \frac{l_{LS2}}{\sqrt{k_2^2+1}}, y_{F_2} = k_2\left(x_{F_2} - x_{E_2}\right) + y_{E_2}. \tag{25}$$

Therefore, the distance between point $F_2$ and line $C_1C_2$ (i.e. $d_2$), can be written as:,

$$d_2 = \frac{x_{F_2} - y_{F_2}}{\sqrt{2}}. \tag{26}$$

In this mechanism, $d_2 \geq 0$ represents that point $F_2$ is below link $C_1C_2$, and vise versa.

The sliding bar $E_2F_2$ is taken as the driving link in the design. To obtain the angle range of the knee joint given in Table 2, the sliding bar $E_2F_2$ should slide along the path defined by the slider at point $D_2$, which will lead to variation of $d_2$. This variation requires that the thigh mechanism should be large enough to provide adequate space. To obtain smaller thigh and knee joint mechanisms, the following conditions should be satisfied: 1) the variation range of $d_2$ should be smaller; 2) the minimal and maximal values of $d_2$ should be restricted in reasonable ranges; 3) the distance between points $E_2$ and $D_2$ (i.e. $d_{LS2}$) should be big enough to provide adequate space for force sensor 2 and the associated parts, and at the same time, it should also be smaller than the length of lead screw 2. In this paper, the second and third conditions are treated as constraints and the objective function is obtained by the first one. Besides, the angle range of the knee joint is also considered in the optimization, and the torque–angle characteristics of the mechanism are used to validate the optimized dimensions.

If $d_{max}^{knee}$ and $d_{min}^{knee}$ represent the maximal and minimal values of $d_2$, respectively, the following constraints can be obtained by the second condition:

$$d_2 \leq d_{max}^{knee} \leq 80, 15 \leq d_{min}^{knee} \leq d_2, \forall\theta_{knee} \in \left[-130^\circ, -10^\circ\right] \tag{27}$$

where the superior limit of $d_{max}^{knee}$ and the inferior limit of $d_{min}^{knee}$ are set by considering the actual dimensions of the associated parts. The third condition can be described by:

$$60 \leq d_{LS2} \leq l_{LS2} - 40, \forall\theta_{knee} \in \left[-130^\circ, -10^\circ\right] \tag{28}$$

where the superior limit of $d_{LS2}$ is obtained by considering the dimension of screw nut 2 and $d_{LS2}$ is defined by:

$$d_{LS2} = \sqrt{\left(x_{E_2} - x_{D_2}\right)^2 + \left(y_{E_2} - y_{D_2}\right)^2}. \tag{29}$$

Therefore, the design variables with their ranges, the objective function, and the constraints can be obtained as follows:

Design vector:

$$\begin{aligned} &\boldsymbol{X}_{knee} = (a_2, b_2, \beta_2) \\ &a_2 \in [a_{21}, a_{22}], b_2 \in [b_{21}, b_{22}], \beta_2 \in [\beta_{21}, \beta_{22}] \end{aligned} \tag{30}$$

Objective function to be minimized:

$$F_2(\boldsymbol{X}_{knee}) = d_{max}^{knee} - d_{min}^{knee} \tag{31}$$

Constraints to be satisfied:

$$d_2 \leq d_{max}^{knee} \leq 80, 15 \leq d_{min}^{knee} \leq d_2, 60 \leq d_{LS2} \leq l_{LS2} - 40, \forall\theta_{knee} \in \left[-130^\circ, -10^\circ\right] \tag{32}$$

where $d_2$ and $d_{LS2}$ are defined by Eqs. (26) and (29), respectively.

The same method as Subsection 2.2 is used to solve the optimization problem defined by Eqs. (30)–(32) by modifying Eqs. (15)–(17), as follows:

$$\boldsymbol{X}_j = \left(x_{j,1}, x_{j,2}, x_{j,3}\right) \tag{33}$$

$$x_{j,0}^d = r_{j,0}^d\left(x_{max}^d - x_{min}^d\right) + x_{min}^d, d = 1, 2, 3 \tag{34}$$

$$v_{j,0}^d = r_j^d\left(x_{max}^d - x_{min}^d\right) + x_{min}^d, d = 1, 2, 3 \tag{35}$$

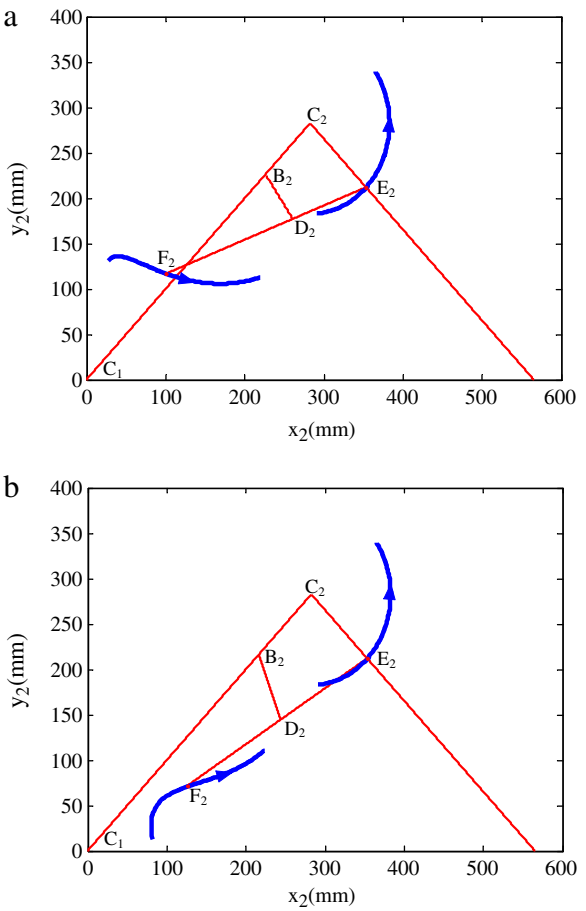


**Fig. 5.** The trajectories of points $F_2$ and $E_2$ when the knee joint angle varies from $-130°$ to $-10°$ with (a) unoptimized dimensions: $a_2 = 80$ mm, $b_2 = 60$ mm and $\beta_2 = 80°$, and (b) optimized dimensions: $a_2 = 94$ mm, $b_2 = 77$ mm and $\beta_2 = 66°$, respectively. The minimum and maximum of distances between point $F_2$ and line $C_1C_2$ are, respectively, $-73.74$ mm and 75.60 mm for (a), and 26.08 mm and 79.56 mm for (b). The minimum and maximum of distances between points $E_2$ and point $D_2$ are, respectively, 31.47 mm and 193.45 mm for (a), and 61.36 mm and 229.99 mm for (b).

where $x_{j,1} \in [a_{21},a_{22}]$, $x_{j,2} \in [b_{21},b_{22}]$ and $x_{j,3} \in [\beta_{21},\beta_{22}]$ represent, respectively, $a_2$, $b_2$ and $\beta_2$; $x^d_{j,0}$, $r^d_{j,0}$, $x^d_{max}$, and $x^d_{min}$ are, respectively, the initial value, a random number generated in range [0, 1], the maximal and minimal values of the $d$th element of the $j$th particle; $v^d_{j,0}$ and $r^d_j$ are the initial value of the $d$th element of $\boldsymbol{V}_j$ and a random number generated in range [0, 1], respectively. The ranges of the elements of $\boldsymbol{X}_j$ and $\boldsymbol{V}_j$ are the same as those of $a_2$, $b_2$ and $\beta_2$, respectively.

In the optimization, the ranges of variables $a_2$, $b_2$ and $\beta_2$ are given by:

$$a_2 \in [80, 120], b_2 \in [60, 100], \beta_2 \in [35^\circ, 105^\circ]. \tag{36}$$

Other parameters of the PSO algorithm for optimization of the knee joint mechanism are the same as Subsection 2.2.

Similar to the hip joint mechanism, there are many solutions satisfying the optimization problem defined by Eqs. (30)–(32). Finally, by considering the torque–angle characteristics, the following optimal solution is selected to be used in this paper: $a_2 = 94$ mm, $b_2 = 77$ mm and $\beta_2 = 66°$.

The trajectories of point $F_2$ with unoptimized and optimized dimensions are shown in Fig. 5(a) and (b), respectively, where the trajectory of point $E_2$ in each subfigure is used to validate that of point $F_2$ as the trajectory of point $E_2$ is a section of a circle obviously. As shown in Fig. 5(a), for the unoptimized dimensions, the distance between point $F_2$ and line $C_1C_2$ varies from $-73.74$ mm, which is inappropriate for this mechanism, to 75.60 mm, such that the range of the distance is 149.34 mm. Whereas, as shown in Fig. 5(b), as for the optimized dimensions, the distance varies from 26.08 mm to 79.56 mm, such that the range is only 53.48 mm, which is much smaller than the former. Furthermore, the minimum of the distance between points $E_2$ and $D_2$ is only 31.47 mm in Fig. 5(a), which is too small for mounting the force sensor 2 and the associated parts.

In this subsection, the output torque of the knee joint mechanism is calculated by setting the force along sliding bar $E_2F_2$ to be 1000 N. The result is given in Fig. 6(a). As a comparison, the relationship between the output torque and knee joint angle when people were doing leg extension obtained in [23] is cited in Fig. 6(b). It is shown that the variation tendency of the output torque of the knee

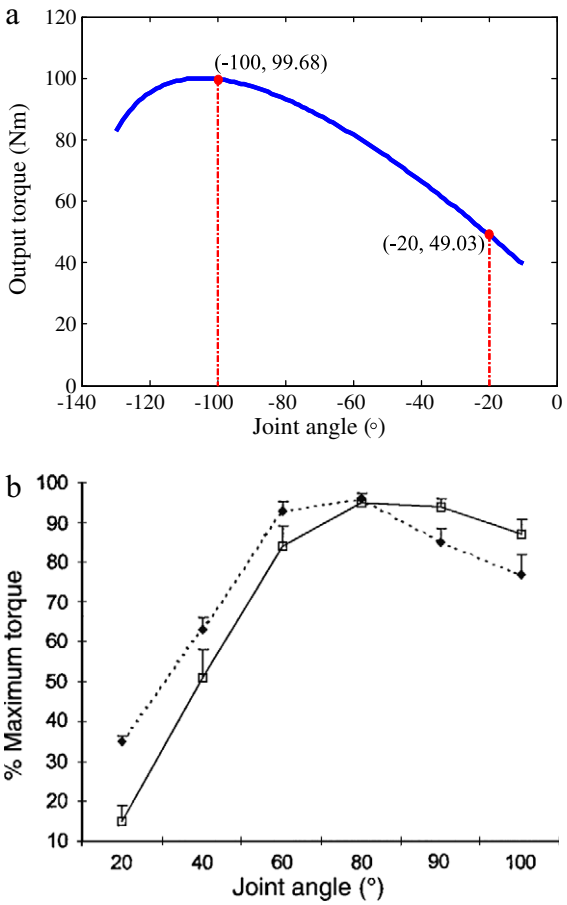


**Fig. 6.** The torque–angle characteristics of (a) the knee joint mechanism, and (b) knee joints of children (□) and adults (♦) [23].

joint mechanism approximately matches that of Fig. 6(b) (It should be noted, although both angles 0° represent full extension, the joint angles in these two subfigures are associated with opposite reference directions. Therefore, as an example, the joint angle − 100° in Fig. 6(a) corresponds to the joint angle 100° in Fig. 6(b)). In addition, it is shown in Fig. 6(a) that the output torque of the knee joint drops about 50.81% (i.e. drops from 99.68 Nm to 49.03 Nm) when the knee joint angle varies from − 100° to − 20°.

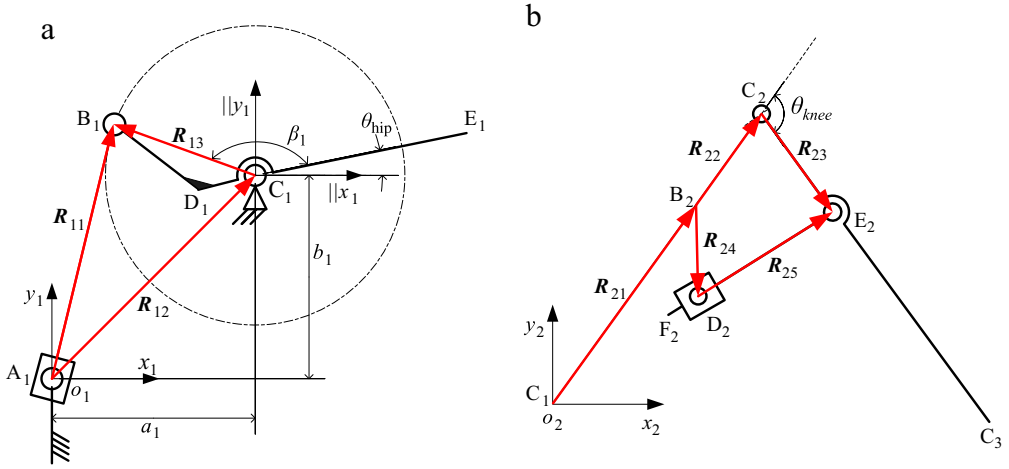


**Fig. 7.** The schematic plots of (a) the hip joint mechanism and (b) the knee joint mechanism.

However, in Fig. 6(b), this drop is bigger (i.e. about 63% for adults and 84% for children). Therefore, the torque–angle characteristics of the knee joint mechanism can satisfy leg extension at least when DC motor 2 is designed according to Table 2 and Fig. 6(a).

## 3. Kinematics

For the leg orthosis proposed in this paper, variation of the ankle joint angle is small and has less effect on the kinematics of the orthosis, such that the crus mechanism and the segment between ankle joint and pedal in Fig. 1 are treated as one link in this paper for simplification. Therefore, the leg orthosis can be taken as a linkage with two links, i.e. thigh and crus links. For each joint mechanism, the ratio of the rotational velocity of associated DC motor to the linear velocity of the lead screw is a constant when the dimensions of the mechanism are determined after optimization. That means, the linear velocity of the lead screw determines uniquely the rotational velocity of the DC motor. Hence, in this paper, the relationships among the displacements and velocities of the lead screws, the hip and knee joints, and the pedal (or the end effector), are considered during the derivation of the kinematics.

For the hip joint mechanism, according to Fig. 7(a), the $x$ and $y$ components of Eq. (3) in Subsection 2.2 can be rewritten, respectively, as:

$$\begin{cases} r_{11}\cos(\theta_{11}) = a_1 + r_{13}\cos\left(\theta_{hip}+\beta_1\right) \\ r_{11}\sin(\theta_{11}) = b_1 + r_{13}\sin\left(\theta_{hip}+\beta_1\right) \end{cases}. \tag{37}$$

The distance between points $A_1$ and $B_1$ (i.e. the linear displacement of lead screw 1) can be derived from Eq. (37), as follows:

$$d_{LS1} = r_{11} = \sqrt{r_{13}^2 + a_1^2 + b_1^2 + 2r_{13}a_1\cos\left(\theta_{hip}+\beta_1\right) + 2r_{13}b_1\sin\left(\theta_{hip}+\beta_1\right)}. \tag{38}$$

By differentiating Eq. (38), the linear velocity of lead screw 1 can be obtained as follows:

$$v_{LS1} = \dot{r}_{11} = \frac{1}{2r_{11}}\left[-2r_{13}a_1\sin\left(\theta_{hip}+\beta_1\right) + 2r_{13}b_1\cos\left(\theta_{hip}+\beta_1\right)\right]\dot{\theta}_{hip}. \tag{39}$$

For the knee joint mechanism, the following vector loop equation can be obtained from Fig. 7(b):

$$\boldsymbol{R}_{22} + \boldsymbol{R}_{23} - \boldsymbol{R}_{24} = \boldsymbol{R}_{25}. \tag{40}$$

The $x$ and $y$ components can be written, respectively, as:

$$\begin{cases} r_{22}\cos\left(\frac{\pi}{4}\right) + r_{23}\cos\left(\theta_{knee}+\frac{\pi}{4}\right) - r_{24}\cos\left(-\frac{3\pi}{4}+\beta_2\right) = r_{25}\cos(\theta_{25}) \\ r_{22}\sin\left(\frac{\pi}{4}\right) + r_{23}\sin\left(\theta_{knee}+\frac{\pi}{4}\right) - r_{24}\sin\left(-\frac{3\pi}{4}+\beta_2\right) = r_{25}\sin(\theta_{25}) \end{cases} \tag{41}$$

where $r_{22} = a_2$, $r_{23} = c_2$ and $r_{24} = b_2$. Therefore, the linear displacement of lead screw 2 can be described by:

$$d_{LS2} = r_{25} = \sqrt{a_2^2 + c_2^2 + b_2^2 + 2a_2c_2\cos(\theta_{knee}) - 2a_2b_2\cos(\beta_2) - 2b_2c_2\cos(\theta_{knee}-\beta_2)}. \tag{42}$$

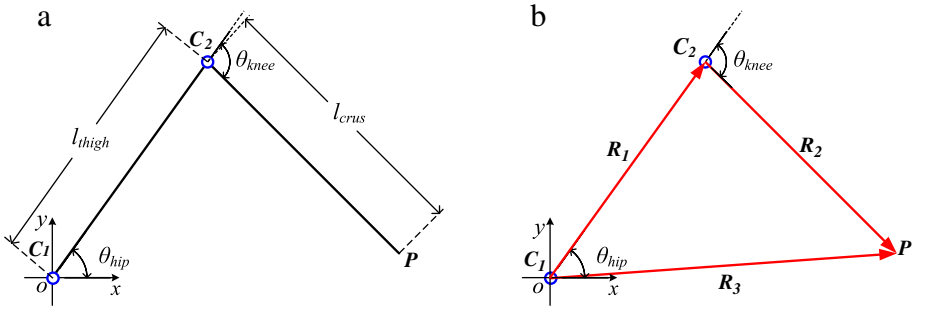


**Fig. 8.** (a) The schematic plot and (b) vector plot for the leg orthosis, where point P denotes the pedal position.

The linear velocity of the lead screw 2 can be obtained by differentiating Eq. (42) as follows:

$$v_{LS2} = \dot{r}_{25} = \frac{1}{2r_{25}}[-2a_2c_2\sin(\theta_{knee}) + 2b_2c_2\sin(\theta_{knee}-\beta_2)]\dot{\theta}_{knee}. \tag{43}$$

In this paper, the leg orthosis is treated as a linkage with two links as is shown in Fig. 8(a), for which the vector plot is given in Fig. 8(b). The following vector loop equation can be obtained from Fig. 8(b):

$$\boldsymbol{R}_1 + \boldsymbol{R}_2 = \boldsymbol{R}_3. \tag{44}$$

The $x$ and $y$ components of Eq. (44) can be described by:

$$\begin{cases} l_{thigh}\cos\left(\theta_{hip}\right) + l_{crus}\cos\left(\theta_{hip}+\theta_{knee}\right) = x_P \\ l_{thigh}\sin\left(\theta_{hip}\right) + l_{crus}\sin\left(\theta_{hip}+\theta_{knee}\right) = y_P \end{cases} \tag{45}$$

where $x_P$ and $y_P$ denote the $x$- and $y$-coordinates of point P, respectively. Both $\theta_{hip}$ and $\theta_{knee}$ can be derived from Eq. (45), as follows:

$$\theta_{hip} = \arctan\left(\frac{y_P}{x_P}\right) + \arccos\frac{l_{thigh}^2 - l_{crus}^2 + x_P^2 + y_P^2}{2l_{thigh}\sqrt{x_P^2+y_P^2}} \tag{46a}$$

$$\theta_{knee} = -\arccos\frac{x_P^2 + y_P^2 - l_{thigh}^2 - l_{crus}^2}{2l_{thigh}l_{crus}}. \tag{46b}$$

Differentiating Eq. (45) gives:

$$\begin{cases} \left[-l_{thigh}\sin\left(\theta_{hip}\right) - l_{crus}\sin\left(\theta_{hip}+\theta_{knee}\right)\right]\dot{\theta}_{hip} - l_{crus}\sin\left(\theta_{hip}+\theta_{knee}\right)\dot{\theta}_{knee} = \dot{x}_p = v_x \\ \left[l_{thigh}\cos\left(\theta_{hip}\right) + l_{crus}\cos\left(\theta_{hip}+\theta_{knee}\right)\right]\dot{\theta}_{hip} + l_{crus}\cos\left(\theta_{hip}+\theta_{knee}\right)\dot{\theta}_{knee} = \dot{y}_p = v_y \end{cases} \tag{47}$$

where $v_x$ and $v_y$ denote the $x$ and $y$ components of the linear velocity of the pedal, respectively. Let

$$\begin{aligned} a_{11} &= -l_{thigh}\sin\left(\theta_{hip}\right) - l_{crus}\sin\left(\theta_{hip}+\theta_{knee}\right), \\ a_{12} &= -l_{crus}\sin\left(\theta_{hip}+\theta_{knee}\right), \\ a_{21} &= l_{thigh}\cos\left(\theta_{hip}\right) + l_{crus}\cos\left(\theta_{hip}+\theta_{knee}\right), \\ a_{22} &= l_{crus}\cos\left(\theta_{hip}+\theta_{knee}\right) \end{aligned}$$

and

$$\theta_{m1} = a_{11}a_{22} - a_{12}a_{21}.$$

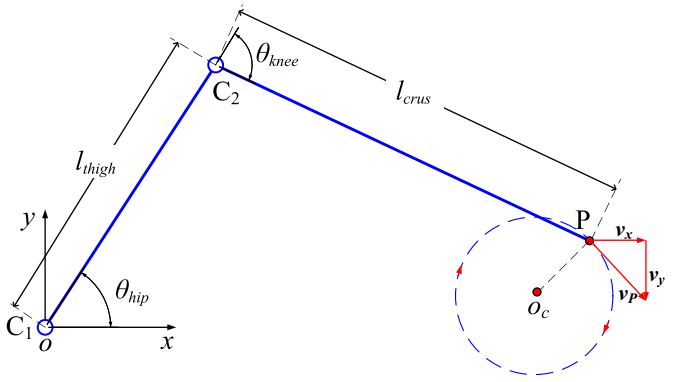


**Fig. 9.** Schematic plot of the cycling exercise. $v_x$ and $v_y$ are the $x$ and $y$ components of $v_P$, the linear velocity of the pedal. The arrows on the circle denote the direction of cycling motion.

The angular velocities of the hip and knee joints can be derived from Eq. (47), as follows:

$$\dot{\theta}_{hip} = \frac{a_{22}v_x - a_{12}v_y}{\theta_{m1}} \tag{48a}$$

$$\dot{\theta}_{knee} = \frac{a_{11}v_y - a_{21}v_x}{\theta_{m1}}. \tag{48b}$$

Therefore, when the position and velocity of point P are given, the angles and the angular velocities of the hip and knee joints can be calculated by Eqs. (46a)–(46b) and (48a)–(48b), respectively. Furthermore, the linear displacements and velocities of lead screws 1 and 2 can be obtained by Eqs. (38), (39), (42) and (43), respectively. As the relationships between the linear displacements and velocities of the lead screws and the pedal are denoted, the kinematics obtained in this section can be used in motion control and trajectory tracking.

## 4. Simulation and discussion

### 4.1. Simulation

In this paper, the cycling exercise, one of the most commonly used and effective ways for lower limb rehabilitation, is considered in simulation to demonstrate the feasibility of the application of the leg orthosis to actual lower limb rehabilitation exercises. The schematic plot of the cycling exercise is given in Fig. 9. It is shown that the trajectory of the pedal (i.e. point P) is a circle centered at point $o_c$, which can be described by:

$$\begin{cases} x_p = x_0 + r\cos(\pi - \omega t) \\ y_p = y_0 + r\sin(\pi - \omega t) \end{cases} \tag{49}$$

where $x_0$ and $y_0$ are, respectively, the $x$- and $y$-coordinates of the center of the trajectory, and $\omega$ is the angular velocity. In this simulation, $x_0$, $y_0$ and $\omega$ are, respectively, set to be 0.65 m, 0.06 m and $0.5\pi$ rad/s. The lengths of the thigh and crus links are set to be 0.385 m and 0.455 m, respectively, where the length of the crus link includes that of the segment between the ankle joint and the pedal. The optimized dimensions obtained in Section 2 and the kinematics obtained in Section 3 are used in the simulation. The simulation time is 8 s.

The simulation of cycling exercise with virtual prototype of the leg orthosis is shown in Fig. 10. Four positions in an exercise cycle are selected. The trajectory of the pedal during the cycling exercise is represented by a blue circle where the red point denotes the position of the pedal. It is shown that during the cycling exercise, the angles of the hip and knee joints and linear displacements of lead screws 1 and 2 vary periodically, which leads to the pedal move by the circular trajectory.

The angles of the hip and knee joints, calculated from Eq. (46a)–(46b), are shown in Fig. 11(a) where the limits for the hip and knee joint angles are given in Table 2. The linear displacements of lead screws 1 and 2, calculated from Eqs. (38) and (42), respectively, are shown in Fig. 11(b) where the limits for the linear displacement of lead screw 2 are the same as those used in the optimization of the knee joint mechanism. It is shown that the angles of the hip and knee joints vary within the ranges given by

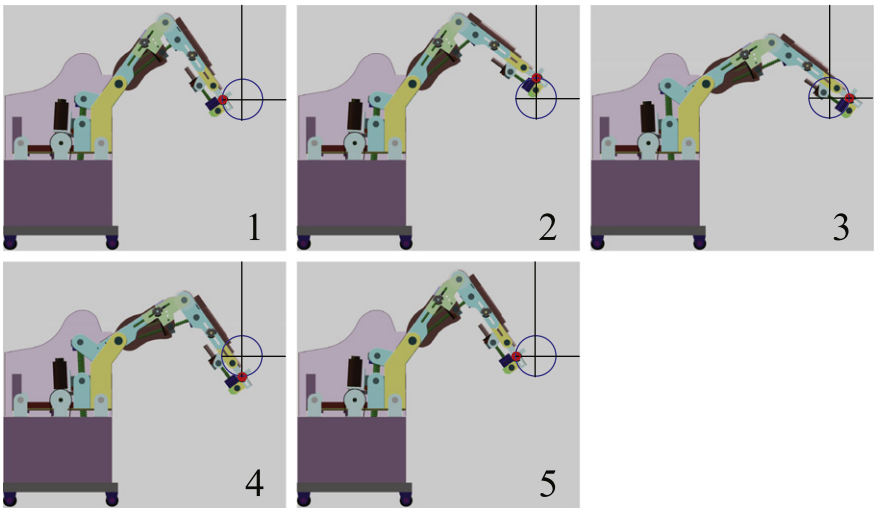


**Fig. 10.** Simulation with the virtual prototype of the leg orthosis.

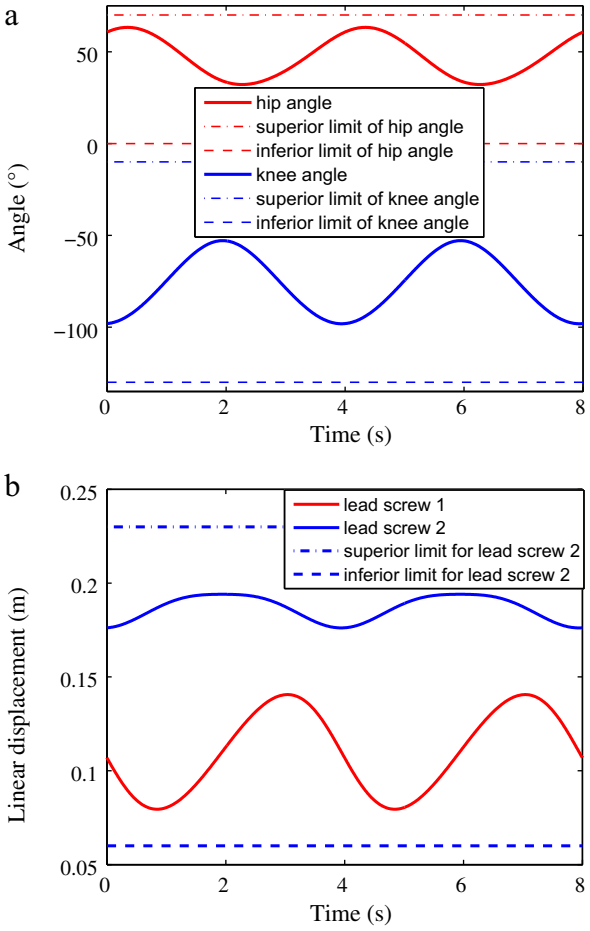


**Fig. 11.** (a) The variation of the hip and knee joint angles, and (b) the linear displacements of lead screws 1 and 2 in the cycling exercise.

Table 2 and the linear displacement of lead screw 2 is in the limits, such that the leg orthosis is applicable for the cycling exercise defined by Eq. (49).

The velocity of the pedal can be obtained by differentiating Eq. (49), as follows:

$$v_x = \omega r \sin(\pi - \omega t), v_y = -\omega r \cos(\pi - \omega t). \tag{50}$$

Therefore, the angular velocities of the hip and knee joints can be obtained by substituting Eq. (50) into Eq. (48a)–(48b) and the linear velocities of lead screws 1 and 2 are obtained by substituting Eq. (48a)–(48b) into Eqs. (39) and (43), respectively. The simulation results are given in Fig. 12. It is shown that the angular velocities of the hip and knee joints and the linear velocities of the lead screws vary periodically in the cycling exercise. Both the amplitudes and variation of the linear velocities of lead screws 1 and 2 are not big and can be easily implemented. Therefore, the leg orthosis proposed in this paper can satisfy the cycling exercise in terms of kinematics, which demonstrates the feasibility of the application to actual lower limb rehabilitation exercises.

### *4.2. Discussion*

In the design proposed in this paper, the force and position sensors are mounted in each joint mechanism. They can be used not only for safety reasons but also for the recognition of the motion intentions of the patients when they are doing exercises with this leg orthosis. Therefore, this orthosis can provide both passive and active exercises, which makes it outperform the devices proposed in [8,12]. ESCM is applied for each joint mechanism and a lead screw and the screw nut are used to constitute the sliding pair. As analyzed in Subsection 2.2, a high transmission ratio can be obtained in this architecture, such that there is no need to include additional speed reducing systems in the joint mechanisms. Hence, the transmission system is more compact than that of the mechanism proposed in [14], which is helpful for the stability of the leg orthosis. As different forms of ESCMs are used for the hip and knee mechanisms, respectively, they can be optimized independently to satisfy different requirements. This design overcomes the deficiencies of the design proposed in [7]. Moreover, different from the joint mechanisms proposed in [7], each of

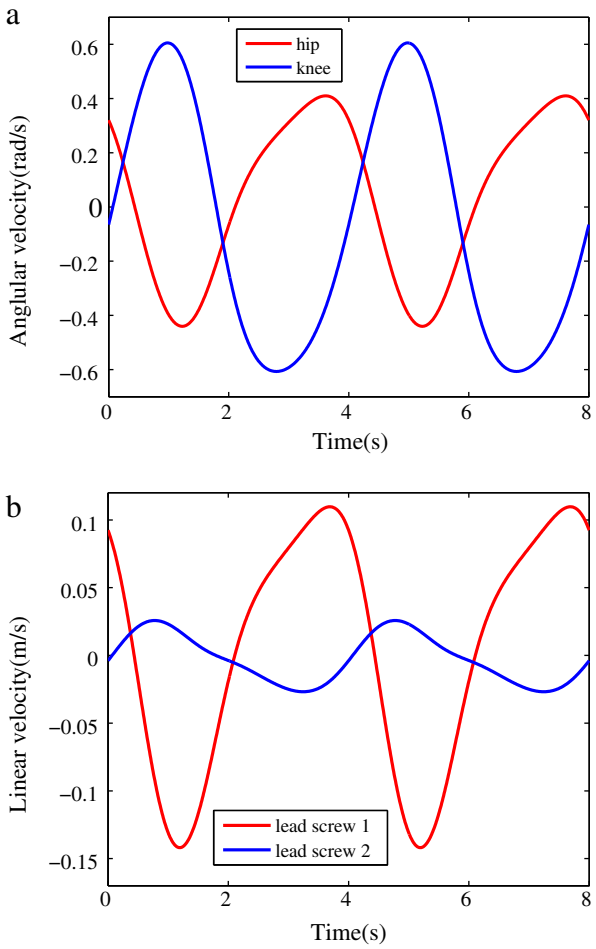


**Fig. 12.** (a) The angular velocities of the hip and knee joints, and (b) linear velocities of lead screws 1 and 2 in the cycling exercise.

the joint mechanisms in this design has unique and stable rotational axis. Since both the lengths of the thigh and crus can be adjusted, each of the rotational axes of the joint mechanisms can be adjusted to exactly match that of corresponding human leg joint, which helps to make the process of rehabilitation exercises more comfortable.

Also, further investigations should be carried out. For example, the relationships between the parameters of rehabilitation exercises and the dimensions of the orthosis should be obtained to ensure the safety and applicability of the orthosis to specific exercises.

## 5. Conclusion

A novel leg orthosis, for LLRR of the sitting/lying type, is proposed in this paper. It consists of three joint mechanisms: hip, knee and ankle, and two sets of links: thigh and crus. By using a lead screw and optimizing the associated dimensions, a high transmission ratio is obtained for each joint mechanism; hence, there is no additional speed reducing systems in the mechanism. This feature makes the transmission system relatively compact and more stable. Each of the rotational axes of the hip, knee and ankle joints is unique and stable, and both of the lengths of the thigh and crus can be adjusted. Thus the hip, knee and ankle joints of the orthosis can be adjusted to exactly match those of human leg. Different forms of ESCMs are respectively used in the three joint mechanisms, consequently, they can be optimized independently. The optimization problems for the hip and knee joint mechanisms are developed respectively, which are characterized as strongly nonlinear. Therefore, a PSO method, which has been proven effective and easier to use for solving nonlinear optimization problems, is used to solve the problems. The obtained solutions are subsequently validated by comparisons between optimized and unoptimized joint mechanisms. Besides, the feasibility of the application of the orthosis to actual rehabilitation exercises is shown by the comparison between the torque–angle characteristics of the knee joint mechanism and that of human knee joint. Furthermore, the kinematics that are necessary for motion control and trajectory tracking are investigated, which denote the relationships between the displacements and velocities of the pedal, the hip and knee joints, and the lead screws. Finally, a simulation example of cycling exercise, one of the

typical lower limb rehabilitation exercises, is formulated to show the feasibility of the application of the leg orthosis to actual exercises. The future work will focus on making the prototype and further investigations of the problems in relation with application.

## Acknowledgment

This research is supported in part by the National Natural Science Foundation of China (Grants 61225017, 61175076), and the International S&T Cooperation Project of China (Grant 2011DFG13390).

## Appendix A. Supplementary data

Supplementary data to this article can be found online at http://dx.doi.org/10.1016/j.mechmachtheory.2013.12.021.

## References

[1] R. Bonita, S. Mendis, T. Truelsen, J. Bogousslavsky, J. Toole, F. Yatsu, The global stroke initiative, Lancet Neurol. 3 (2004) 391–393.
[2] S.T. Pendlebury, Worldwide under-funding of stroke research, Int. J. Stroke 2 (2007) 80–84.
[3] M. Wyndaele, J.J. Wyndaele, Incidence, prevalence and epidemiology of spinal cord injury: what learns a worldwide literature survey? Spinal Cord 44 (2006) 523–529.
[4] X. Li, E.J. Curry, M. Blais, R. Ma, A.S. Sungarian, Intraspinal penetrating stab injury to the middle thoracic spinal cord with no neurologic deficit, Orthopedics 35 (5) (2012) e770–e773.
[5] M. Pohl, C. Werner, M. Holzgraefe, G. Kroczek, I. Wingendorf, G. Hölig, R. Koch, S. Hesse, Repetitive locomotor training and physiotherapy improve walking and basic activities of daily living after stroke: a single-blind, randomized multicentre trial (DEutsche GAngtrainerStudie, DEGAS), Clin. Rehabil. 21 (2007) 17–27.
[6] G. Kwakkel, B.J. Kollen, H.I. Krebs, Effects of robot-assisted therapy on upper limb recovery after stroke: a systematic review, Neurorehabil. Neural Repair 22 (2) (2008) 111–121.
[7] C. Schmitt, P. Métrailler, A. Al-Khodairy, R. Brodard, J. Fournier, M. Bouri, R. Clavel, The Motion Maker™: a rehabilitation system combining an orthosis with closed-loop electrical muscle stimulation, Proceedings of the 8th Vienna International Workshop on Functional Electrical Stimulation, Vienna, Austria, 2004, pp. 117–120.
[8] M. Bouri, B. Le Gall, R. Clavel, A new concept of parallel robot for rehabilitation and fitness: the Lambda, Proceedings of the 2009 IEEE International Conference on Robotics and Biomimetics, Guilin, China, 2009, pp. 2503–2508.
[9] G. Colombo, M. Joerg, R. Schreier, V. Dietz, Treadmill training of paraplegic patients using a robotic orthosis, J. Rehabil. Res. Dev. 37 (6) (2000) 693–700.
[10] S. Freivogel, J. Mehrholz, T. Husak-Sotomayor, D. Schmalohr, Gait training with the newly developed '®LokoHelp'-system is feasible for non-ambulatory patients after stroke, spinal cord and brain injury: a feasibility study, Brain Inj. 22 (7–8) (2008) 625–632.
[11] Y. Stauffer, Y. Allemand, M. Bouri, J. Fournier, R. Clavel, P. Metrailler, R. Brodard, F. Reynard, The WalkTrainer—a new generation of walking reeducation device combining orthoses and muscle stimulation, IEEE Trans. Neural Syst. Rehab. Eng. 17 (1) (2009) 38–45.
[12] K. Kong, C. Baek, M. Tomizuka, Design of a rehabilitation device based on a mechanical link system, Proceedings of the 2009 IEEE International Conference on Robotics and Automation, Kobe, Japan, 2009, pp. 2306–2311.
[13] M. Lotze, C. Braun, N. Birbaumer, S. Anders, L.G. Cohen, Motor learning elicited by voluntary drive, Brain 126 (2003) 866–872.
[14] X.H. Shi, H.B. Wang, L. Yuan, Z. Xu, H.W. Zhen, Z.G. Hou, Design and analysis of a lower limb rehabilitation robot, Adv. Mater. Res. 490–495 (2012) 2236–2240.
[15] P. Metrailler, V. Blanchard, I. Perrin, R. Brodard, R. Frischknecht, C. Schmitt, J. Fournier, M. Bouri, R. Clavel, Improvement of rehabilitation possibilities with the Motion Maker™, Proceedings of the 1st IEEE RAS & EMBS International Conference on Biomedical Robotics and Biomechatronics (BioRob 2006), New York City, USA, 2006, pp. 359–364.
[16] H.Y. Sun, L.X. Zhang, X.P. Hu, L.H. Tian, Experiment study of fuzzy impedance control on horizontal lower limbs rehabilitation robot, Proceedings of the 2011 International Conference on Electronics, Communications and Control (ICECC 2011), Ningbo, China, 2011, pp. 2640–2643.
[17] J. Kennedy, R. Eberhart, Particle swarm optimization, Proceedings of the 1995 IEEE International Conference on Neural Network, Perth, Australia, 1995, pp. 1942–1948.
[18] R. McDougall, S. Nokleby, Synthesis of Grashof four-bar mechanisms using particle swarm optimization, Proceedings of the 2008 International Design Engineering Technical Conferences & Computers and Information in Engineering Conference, Brooklyn, New York, USA, 2008, pp. 1–5.
[19] V. Savsani, R.V. Rao, D.P. Vakharia, Optimal weight design of a gear train using particle swarm optimization and simulated annealing algorithms, Mech. Mach. Theory 45 (3) (2010) 531–541.
[20] A. Macor, A. Rossetti, Optimization of hydro-mechanical power split transmissions, Mech. Mach. Theory 46 (12) (2011) 1901–1919.
[21] Y.C. Lin, M.J.J. Wang, E.M. Wang, The comparisons of anthropometric characteristics among four peoples in East Asia, Appl. Ergon. 35 (2) (2004) 173–178.
[22] R. Eberhart, J. Kennedy, A new optimizer using particle swarm theory, Proceedings of the Sixth International Symposium on Micro Machine and Human Science, Nagoya, Japan, 1995, pp. 39–43.
[23] V. Marginson, R. Eston, The relationship between torque and joint angle during knee extension in boys and men, J. Sports Sci. 19 (11) (2001) 875–880.